The International Journal of Advanced Manufacturing Technology (2023) 126:1279–1292
https://doi.org/10.1007/s00170-023-11158-x

ORIGINAL ARTICLE

Experimental analysis on the influence of the tool micro geometry on the wear behavior in gear hobbing

Felix Kühn[1] · Steffen Hendricks[1] · Nico Troß[1] · Jens Brimmers[1] · Thomas Bergs[1,2]

Received: 12 August 2022 / Accepted: 23 February 2023 / Published online: 9 March 2023

Abstract

Gear hobbing is a well-established manufacturing process for cylindrical spur gears. The cutting edge of a hobbing tool is, among others, characterized by the cutting edge radius and the form-factor K. The magnitude of these parameters is ideally chosen based on the machining conditions given by the workpiece and cutting material and the cutting parameters as well as the gear and tool geometry. However, the influence of the cutting edge geometry on tool life and wear behavior is hardly known, which complicates an optimized tool design. Furthermore, the preparation process regarding the coating thickness distribution on the wear behavior is equally relevant. Therefore, the objective was to identify the influence of the cutting edge radius, the form-factor K, and the preparation process on the wear behavior of gear hobbing tools made of powder metallurgical high-speed steel (PM-HSS). Fly-cutting trials were performed as an analogy process for gear hobbing in order to study the wear behavior and identify the respective tool lives. The trials indicated that the form-factor K influences the wear behavior, while a variation of the cutting edge radius did not have a significant effect. A homogenous coating thickness could extend the tool life significantly.

Keywords Gear hobbing · Tool microgeometry · Cutting edge radius · Form-factor K · Tool wear · Fly-cutting trial

1 Introduction and objective

In cutting processes, the tool cutting edge is subject to high loads. These loads lead to wear on the tool, which determines the productivity of the process and the manufactured component surface quality. The shape and sharpness of the cutting edge is of decisive importance. Productivity and process reliability can therefore be increased by a knowledge-based design of the tool cutting edge.

For turning operations, the influence of the tool microgeometry on the tool wear was studied in detail by Basset and Denkena [2, 9, 10]. Basset deducted tool life maps for different workpiece materials, in which the influence of the tool microgeometry on the tool life was shown. TiAlN-coated carbide K30F inserts were used as tools. The applied cutting speeds were in the range of $v_c = 60$ m/min to 300 m/min at a constant maximum uncut chip thickness of $h_{cu,max} = 0.2$ mm. Basset observed that the tendency for crater wear increased for form-factors $K > 1$, while the tendency for flank wear increased for $K < 1$. An optimum cutting edge radius of $r_\beta = 25$–30 µm regarding wear resistance was determined. The results of Basset are consistent with the results of Enders, who investigated the influence of the cutting edge radius on tool wear during external cylindrical turning of C45E [13]. Deng showed that increasing the cutting edge radius up to a certain point leads to a reduction in initial wear and an increase in tool life [8]. Other studies on the tool microgeometry in turning were carried out by Coelho [7], Shintani [28], Denkena [11, 12], Özel [15, 22, 24, 25], Ventura [32], Al-Zkeri [1], Wyen [34], Fang [14], and Bergmann [3], among others. Due to the complex chip formations resulting from the multi-flank chip formation and the interrupted cut in gear hobbing, the results from turning cannot be transferred directly to gear hobbing.

The hobbing process has been studied many times in the past regarding tool wear. Most of the studies used the parameters resulting from the process data and the macrogeometry of the workpiece and hob for wear prediction. Especially the chip length and the chip thickness were used [5].

✉ Steffen Hendricks
s.hendricks@wzl.rwth-aachen.de

[1] WZL of RWTH Aachen University, Campus-Boulevard 30, 52074 Aachen, Germany

[2] Frauenhofer IPT, Steinbachstraße 17, 52074 Aachen, Germany

Karpuschewski used an FE analysis to explain the occurring wear phenomena when machining with carbide hobs [18]. He also investigated the influence of various tool macrogeometry parameters on the tool wear during hobbing [17]. Kühn investigated the influence of the effective tool angles on the wear behavior [19].

For gear hobbing, only few investigations on the influence of the cutting edge geometry on the tool wear have been reported. Lux used the fly-cutting trial as an analogy process to gear hobbing and investigated the influence of the cutting edge radius on the wear behavior. He carried out experiments with three different process parameter variations: $v_c = 80$ m/min and $h_{cu,max} = 0.3$ mm; $v_c = 80$ m/min and $h_{cu,max} = 0.33$ mm; $v_c = 120$ m/min and $h_{cu,max} = 0.3$ mm. For all process variations, cutting edge radii of $r_\beta = 15$ µm, $r_\beta = 30$ µm, and $r_\beta = 50$ µm were applied with a brass brush. In all trials, a larger cutting edge radius resulted in increased flank wear and thus a shorter tool life [20].

Winkel reported on the influence of the cutting edge radius on the wear behavior of TiAlN-coated K20 carbide fly-cutters. When machining 20 MnCrS5 case-hardening steel, the initial wear was significantly reduced by applying a radius of $r_\beta = 15$ µm compared to an almost ideally sharp tool with $r_\beta \approx 0$ µm. In addition, an optimum range of cutting edge radius of $r_\beta = 10$–15 µm was found in fly-cutting trials. In particular, abrasive flank wear was reduced by an optimum cutting edge radius. The reasons given were a better coating resistance and less cutting edge chipping [33].

In addition to Winkel and Rech carried out investigations for optimized cutting edge radius. In the trials, TiAlN-coated S290 tools were used with two different preparation processes: flow grinding and sandblasting. The ground tools achieved higher tool life than the sandblasted tools. The cutting edge radius was varied from $r_\beta = 5$ µm to $r_\beta = 30$ µm. A tool life-optimized cutting edge radius was identified at $r_\beta = 15$ µm to $r_\beta = 20$ µm [26].

The compiled results regarding the influence of the cutting edge microgeometry on the cutting process confirm the high potential of cutting edge preparation to increase the tool life. Lux [20], Winkel [33], and Rech [26] only carried out investigations on the influence of the cutting edge radius on the wear behavior. Asymmetrical cutting edges with different form-factors K have not yet been investigated for hobbing.

It was shown that not only the influence of the cutting edge geometry on the wear behavior is of decisive importance for the performance of a hob cutting edge, but also the influence of the preparation process on the wear behavior [7]. Therefore, the objective of this report is to review the findings from other processes in hobbing and, building on the studies already conducted in hobbing, to identify the influence of the cutting edge radius, the form-factor K, and the preparation process on the wear behavior for hobbing with PM-HSS tools with AlCrN coating. The focus is on the interaction of the tool microgeometry with the coating thickness and its influence on the tool wear. An important factor that has not been investigated in detail before is the coating thickness distribution, which results from the PVD coating process. For this purpose, the cutting edge radius, the form-factor K, and the preparation process are varied. In fly-cutting trials, the influence of the variation parameters on the tool wear is investigated.

2 Materials and methods

2.1 Workpiece geometry and material

The gear used for the experiments is shown in Table 1. The workpiece has a normal module of $m_{n2} = 2.557$ mm, a number of teeth of $z_2 = 39$, a pressure angle of $\alpha_{n2} = 17.5°$, a helix angle of $\beta_2 = 23°$, and a tip diameter of $d_{a2} = 116.2$ mm. The material used was case-hardened steel 18CrNiMo7-6. The gear geometry is based on a typical automotive crankshaft gear.

Figure 1 shows a micrograph of the workpiece material microstructure. The material 18CrNiMo7-6 had a ferritic-pearlitic microstructure. The chemical composition of the material, shown in Table 2, was determined by optical emission spectrometry (OES). An indentation hardness of 160 HV30 was measured on the material surface, which corresponds to a tensile strength of $R_m = 510$ MPa according to DIN EN ISO 18265 [21]

2.2 Tool geometry and preparation

The trials were performed using the fly-cutting process as analogy process to gear hobbing. Fly-cutting trials have already been used in several investigations [4, 16, 27]. The tool data are shown in Table 3. The tools used in these investigations were double-start, right-handed hobs with an outer diameter

Table 1 Gear geometry

	Symbol	Value	Unit
Material		18CrNiMo7-6	-
Normal module	m_{n2}	2.557	mm
Number of teeth	z_2	39	-
Pressure angle	α_2	17.5	°
Tip diameter	d_{a2}	116.2	mm
Helix angle	β_2	23	°
Gear width	b_2	30	mm
Generating profile shift coefficient	x_{E2}	0.0557	-
Root diameter	d_{f2}	100	mm

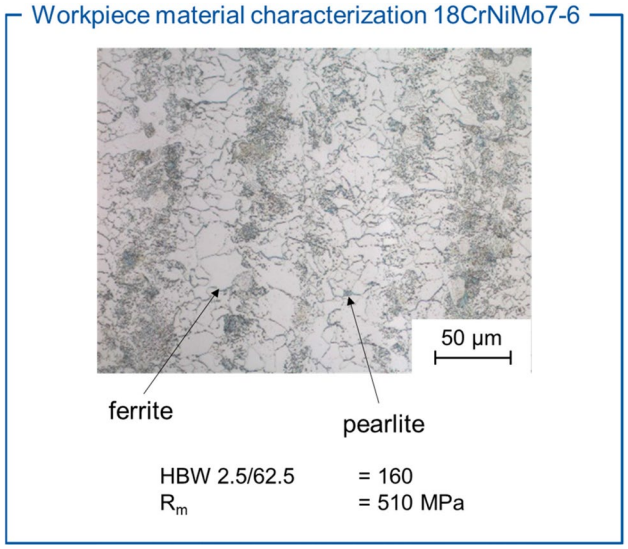

Fig. 1 Workpiece material characterization

of $d_{a0}=80$ mm, a number of gashes of $n_{i0}=17$, and a module of $m_{n0}=2.557$ mm. The cutting substrate was a powder metallurgical high-speed steel (PM-HSS) S390, which was initially coated with AlCrN.

The required fly-cutting tools were segmented from a common hob by wire erosion. After segmentation, the tools were de-coated and ground. The cutting edge was then treated by abrasive stream grinding. In this process, an abrasive fluid flows around the cutting edge. The cutting edge geometry can then be adjusted by changing the process setting like time, pressure, pressure change, and impact angle. After preparation, all fly-cutters were coated in the same batch with AlCrN. Figure 2 shows the SEM micrographs after the different preparation steps. In the uncoated, unprepared state, the cutting material appears brittle. The machining marks from the grinding process are clearly visible on the rake face and the flank. The cutting edge appears very sharp due to a low cutting edge radius. After abrasive stream grinding, the cutting edge radius was increased. The rounding is homogeneous along the cutting edge, and the machining marks from the grinding process are barely visible. After the coating process, the cutting edge rounding still appeared homogeneous. No further process steps were carried out to increase the coating quality, as, for example, in other studies [6]. The coating thickness was constant over the radius. White spots were observed on the tool, which can be attributed to coating defects. Since these defects only occurred in isolated cases on the surface, the tool quality was considered to be suitable for the experiments. All tools were examined optically at the beginning of the trials to ensure that only defect-free tools were used.

The initial state of the tool is documented in Fig. 3. The roughness and coating thickness of the rake face and the clearance flanks (LF and TF) as well as the cutting edge roughness are shown. The coating thickness was $s=2.25$ µm on the rake face and $s=1.63$ µm or $s=1.94$ µm on the clearance flanks. All values correspond to standard industrial values.

The fly-cutters, which are listed in the experimental design under the wet blasting preparation process, were used in the cutting trials after segmentation from the hob. The cutting edge preparation was carried out during the normal production process of the hob by the tool manufacturer using wet blasting. The wet blasting process is similar to the abrasive stream grinding process. However, in the wet process, the abrasive fluid is directed through a nozzle with compressed air onto the cutting edge. Thus, the fly-cutters, which were prepared by wet blasting, were not coated in the same batch as the fly-cutters prepared by abrasive stream grinding. However, the specification of the coating was identical.

2.3 Design of experiments

The tool wear investigations were carried out on a Liebherr LC180 hobbing machine. The fly-cutting process kinematic and the trial setup are shown in Fig. 4. In addition, a detailed view of a fly-cutter is shown on the right side of the image. For each trial the wear mark width was measured at the marked areas. The areas were divided into the leading flank LF-B, the transition of the leading flank to the tip LF-A, the tip T, the transition of the trailing flank to the tip TF-A, and the trailing flank TF-B. As wear criteria, a maximum permissible wear mark width of $VB_{max,perm}=150$ µm and a maximum permissible crater depth of $KT_{max,perm}=100$ µm

Table 3 Tool data

	Symbol	Value	Unit
Cutting material, coating		S390, AlCrN	-
Normal module	m_{n0}	2.557	mm
Tip diameter	d_{a0}	80	mm
Number of starts	z_0	2, right	-
Number of gashes	n_{i0}	17	-
Tip radius	ρ_{aP0}	0.85	mm

Table 2 Chemical composition

w-%	C	Si	Mn	P	S	Cr	Mo	Ni
Actual condition	0.207	0.246	0.526	0.0063	0.0028	1.64	0.3292	1.5
DIN EN 10084	0.15–0.21	≤0.4	0.5–0.9	≤0.025	≤0.035	1.5–1.8	0.25–0.35	1.4–1.7

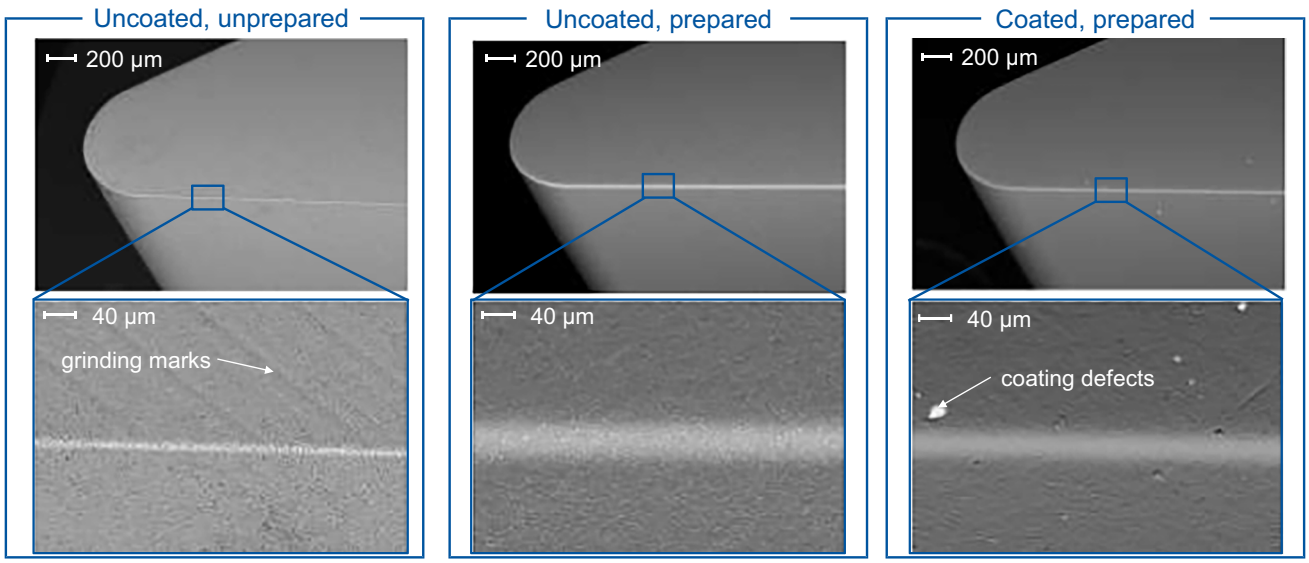

Fig. 2 SEM micrographs of individual preparation steps of the tools

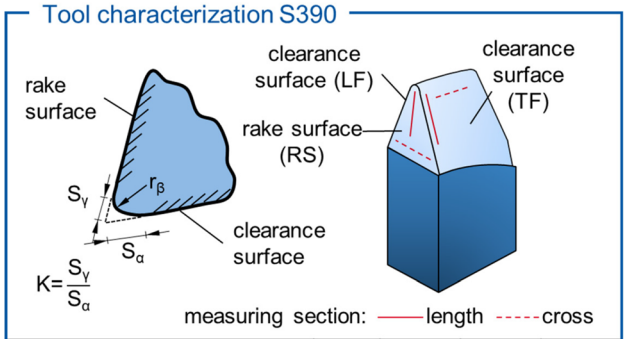

		LF	RS	TF
roughness (Ra - length)	[µm]	0.20	0.17	0.27
roughness (Ra - cross)	[µm]	0.18	0.15	0.18
roughness (Rz - length)	[µm]	1.51	1.17	1.95
roughness (Rz - cross)	[µm]	1.29	1.21	1.41
cutting edge roughness (Rz)	[µm]	1.31	-	1.35
coating thickness	[µm]	1.63	2.25	1.94

Fig. 3 Tool characterization

were chosen. The wear criteria were adopted from previous studies [17, 28] which showed that exponential wear growth starts at these wear mark widths.

To investigate the influence of the cutting edge radius, the form-factor K, and the preparation process on the wear behavior, the experiments were designed according to Fig. 5. The tool microgeometry variation was introduced by the preparation process abrasive stream grinding. The corresponding trials were carried out with a cutting speed of $v_c = 200$ m/min and a feed rate of $f_a = 2.5$ mm, which corresponds to a maximum uncut chip thickness of $h_{cu,max} = 0.2$ mm. All trials were conducted without cutting fluid. In this trial, the cutting edge radius and the form-factor K were examined full factorial within the manufacturing limits. The cutting edge radius was $r_\beta = 10$ µm, $r_\beta = 18$ µm, $r_\beta = 22$ µm, and $r_\beta = 30$ µm and the form-factor $K = 0.3$, $K = 1$, and $K = 3$.

In addition, the influence of the preparation process was examined for tools with $r_\beta = 22$ µm and $K = 1$ for two different cutting speeds $v_c = 150$ m/min and $v_c = 200$ m/min. The wet-blasted fly-cutters used were segmented from a hob. The abrasive stream ground fly-cutters were first separated, de-coated, and then rounded and coated. In contrast to the coating of individual cutter teeth, shading effects occur when coating the entire hob. Shading effects occur when the tool surface is not freely accessible from all directions. These effects lead to different coating thicknesses over the tool profile. Therefore, the results were mainly examined with regard to the coating thickness distribution.

2.4 Measuring strategy for the characterization of the cutting edge microgeometry

The profile of the cutting edge geometry was documented by means of tactile measurement at five positions on the leading flank, three at the tip, and five on the trailing flank; see Fig. 6. More measuring positions were defined at the wear-critical area at the tip and at the transition from the tip to the leading and trailing flanks. The advantage of a tactile measurement compared to an optical is that information about the cutting edge radius, the shape of the cutting edge, and the amount of wear can be determined even on worn cutting edges. Optical measuring systems showed deficiencies in the evaluation of worn cutting edges. Often, the system

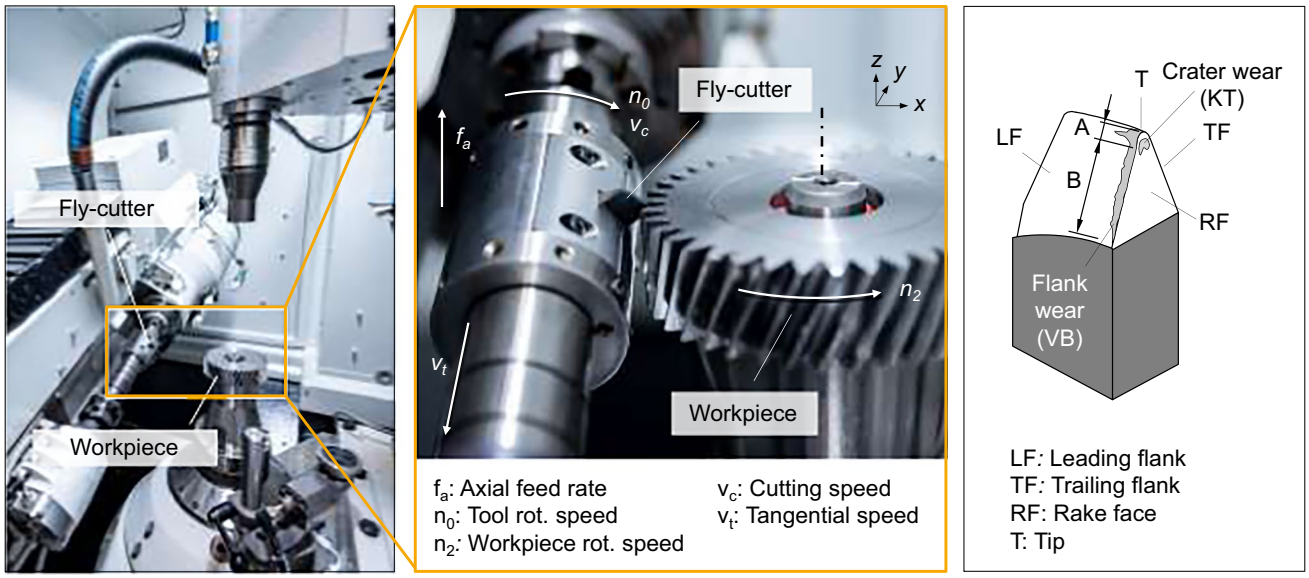

Fig. 4 Experimental setup

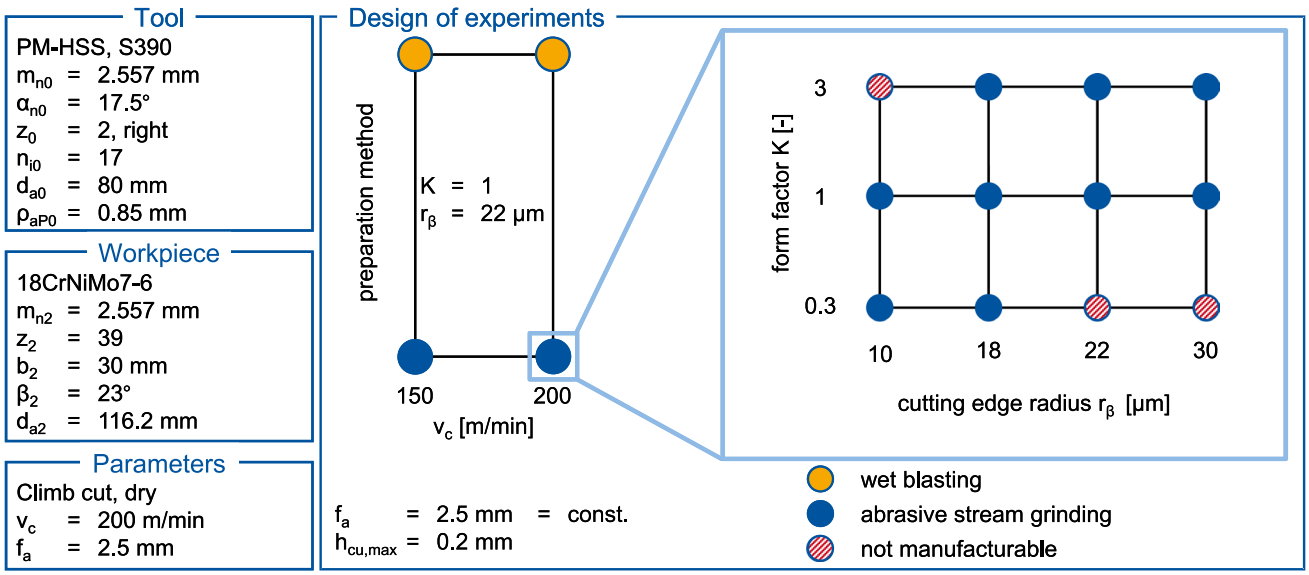

Fig. 5 Design of experiments

did not identify the correct edge, so that it was not possible to characterize the cutting edge.

3 Wear investigations in fly-cutting trials

3.1 Influence of the preparation process on the wear behavior

The trials were carried out for each preparation process at two different cutting speeds $v_c = 150$ m/min and $v_c = 200$ m/min. The axial feed was kept constant at $f_a = 2.5$ mm for all trials. The workpieces were manufactured in climb cut and without cooling lubricant. For each fly-cutter, the maximum flank wear VB_{max} and the maximum crater depth KT_{max} for different areas along the tool profile were plotted over the machined length L; see Fig. 7. The machined length is the product of the number of teeth z_2 and the width b_2 of the workpiece divided by the cosine of the helix angle β_2. The tool life LT is defined as the machined length after the tool wear has reached one of the wear criteria $VB_{max,perm.}$ or $KT_{max,perm.}$.

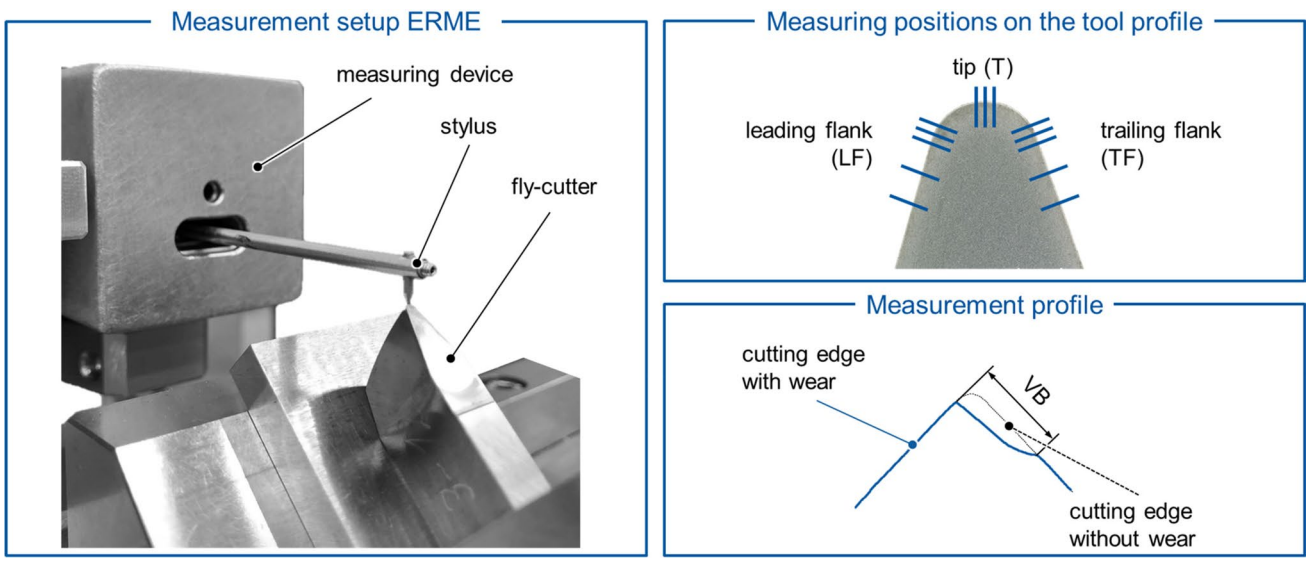

Fig. 6 Measuring strategy for the characterization of the tool micro geometry

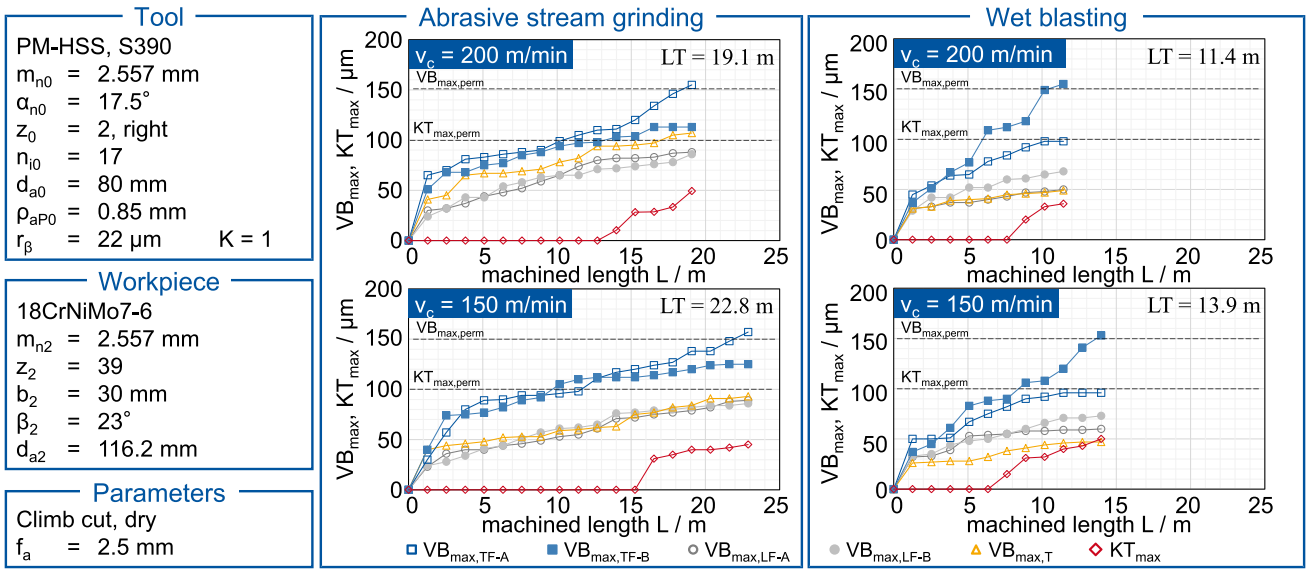

Fig. 7 Wear curves of the differently prepared fly-cutters

The abrasive stream ground fly-cutters reached the wear criterion due to flank wear in the TF-A area. With a cutting velocity of $v_c = 200$ m/min, a tool life of LT = 19.1 m was achieved, and with a cutting velocity of $v_c = 150$ m/min, a tool life of LT = 22.8 m was achieved. The wet-blasted fly-cutters reached the wear criterion due to flank wear in area TF-B after a tool life of LT = 11.4 m with $v_c = 200$ m/min and a tool life of LT = 13.9 m with $v_c = 150$ m/min. The characteristics of the wear curves at TF-A are comparable for abrasive stream ground and wet-blasted fly-cutters. The wear in the TF-A area is typical for HSS tools in the given process, since the largest chip lengths occur in this area [31]. Crater wear occurred on all fly-cutters. The crater initiation occurred earlier for the wet-blasted fly-cutters than for the abrasive stream ground fly-cutters.

The wear criterion was achieved by flank wear in different areas of the cutting edge. Especially the lower area of the trailing flank TF-B was not classified as wear-critical in previous research [30, 31]. For this reason, further analyses were carried out. Figure 8 compares the wear images of the trailing flank after reaching the wear criterion. The amount of wear of the wet-blasted fly-cutters increases continuously from tip to root until the largest amount of wear in the lower area occurs on the trailing flank. The flank wear of the

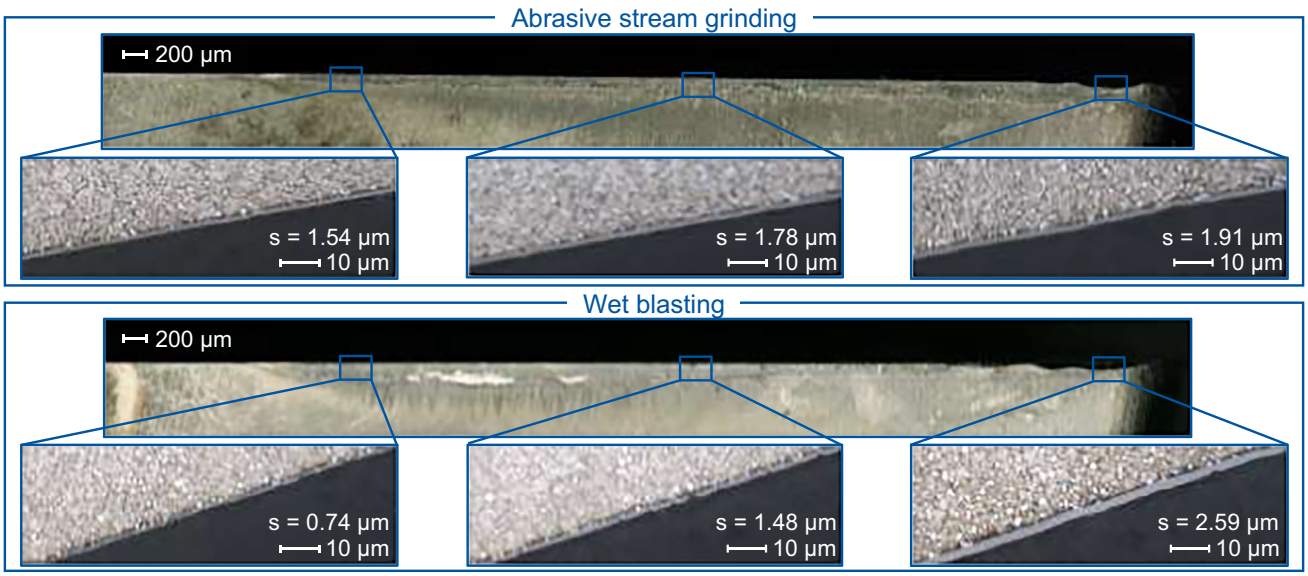

Fig. 8 Wear and coating thickness analysis

abrasive stream ground fly-cutters did not show this amount of wear. At the abrasive stream ground fly-cutters, the wear of the flank increased from the root towards the tip.

To analyze the different wear behavior along the flank, the coating thickness of the fly-cutters was analyzed. The micrographs of the coating thickness in Fig. 8 were taken in the unused condition of the tool. The coating thickness of the abrasive stream ground fly-cutters had a comparable coating thickness of $s = 1.54$ µm to $s = 1.91$ µm along the entire tool profile. On the wet-blasted fly-cutters, the coating thickness decreased significantly from the tip towards the root until there is only a coating thickness of $s = 0.74$ µm in the lower area of the profile. This effect results from the line of sight characteristic of the PVD coating process. The coating process of a full hob results in the highest coating thicknesses at the tip. The coating thickness decreases at the clearance flank towards the root. The accessibility in the tooth root and the shading effects of adjacent teeth reinforce this effect. The analysis of the coating thickness provided an explanation for the unusual wear behavior. It was also shown that a uniform coating thickness is important for the achievable tool life.

3.2 Influence of the cutting edge radius r_β on the wear behavior

In this section the influence of the cutting edge radius r_β on the wear behavior of fly-cutters is analyzed. For this purpose, fly-cutters with different cutting edge radii were prepared by abrasive stream grinding. The measured cutting edge radii were classified into $r_\beta = 10$ µm, $r_\beta = 18$ µm, $r_\beta = 22$ µm, and $r_\beta = 30$ µm after the coating process. The form-factor was symmetric for all tools with $K = 1$. For the fly-cutters with a cutting edge radius of $r_\beta = 10$ µm, $r_\beta = 22$ µm, and $r_\beta = 30$ µm, the initial condition of the tools was documented with SEM micrographs; see Fig. 9. Several fly-cutters were prepared for the respective tool microgeometry in the same batch, and the coating was also applied to all tools in the same batch. Thus, the initial conditions for the respective tool microgeometry are comparable. The different cutting edge radii are clearly visible in the images. All tools have a homogeneous and defect-free cutting edge along the entire tool profile. In some cases, small coating defects in the form of small white dots are visible on the rake face and flank. However, the tool defects did not occur over a large area and only occurred with a low frequency. Therefore, the tools were used in the trials.

Figure 10 shows the wear curves for the different cutting edge radii. For each fly-cutter, the maximum flank wear VB_{max} and the maximum crater depth KT_{max} for different areas along the tool profile were plotted over the machined length L. The process parameters were kept constant with $v_c = 200$ m/min and $f_a = 2.5$ mm. Machining took place without cooling lubricant.

The characteristics of the wear curves are comparable for the fly-cutters with different cutting edge radii. At the beginning of the cutting process, an initial wear of $VB_{max} \approx 50$ µm occurred. This was followed by a linear uniform increase in wear up to a machined length of $L = 16.5$ m, from which the exponential wear range or exceeding of the wear criterion was reached. The wear criterion was reached after a machined length of $L_{r\beta=10} = 20.3$ m, $L_{r\beta=18} = 17.8$ m, $L_{r\beta=22} = 19.1$ m, and $L_{r\beta=30} = 17.8$ m. For all tools, the wear criterion was achieved by flank wear at area TF-A. Also, the distribution of the wear on the trailing flank, the tip area,

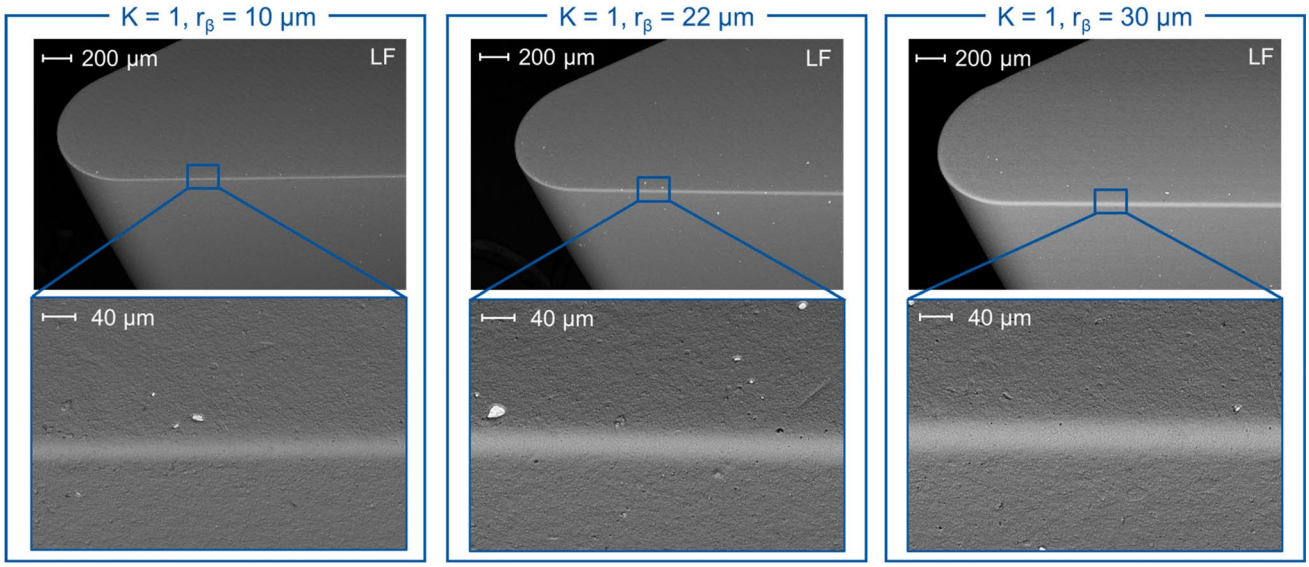

Fig. 9 Initial condition of fly-cutters with different cutting edge radii r_β

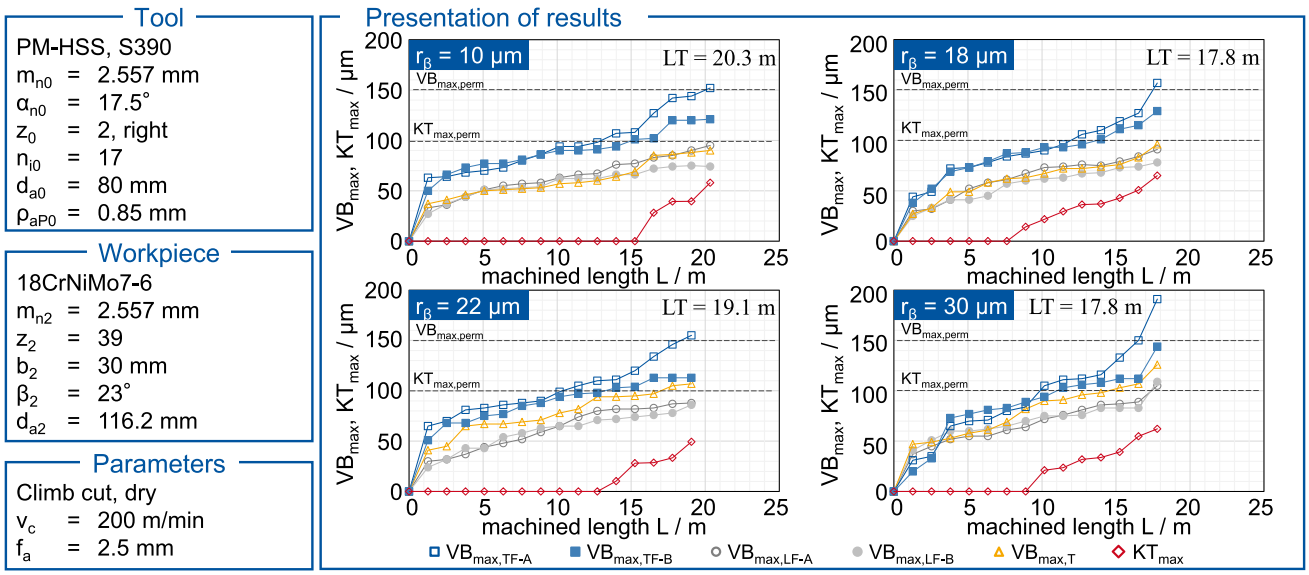

Fig. 10 Wear curves for variation of the cutting edge radius r_β

and the leading flank was comparable for all tools. The lowest wear always occurred on the leading flank. Crater wear occurred for all tools on the rake face in the TF-A area, but did not lead to tool failure. Based on the wear curves, no clear influence on the wear behavior of the fly-cutters could be observed by varying the cutting edge radius. Effects of higher wear due to higher tool loads with larger cutting edge radii, which were demonstrated by Ozturk [23], could not be observed.

Figure 11 shows the tactile measurement of the cutting edge of the tool with $r_\beta = 22$ µm and $K = 1$. The cutting edge was measured at five positions. On the left, the tool is shown in its initial state. The cutting edge radii and form-factors vary only slightly over the five positions. After $L = 10.2$ m machined length, the cutting edge is recessed at all positions due to flank wear along the entire tool profile. With the exception of the tip area, the cutting edge radii have significantly smaller values than at the beginning. The form-factors also change significantly in some cases. At position 2, the form-factor is doubled, while it drops from $K = 1.1$ to $K = 0.4$ at position 5.

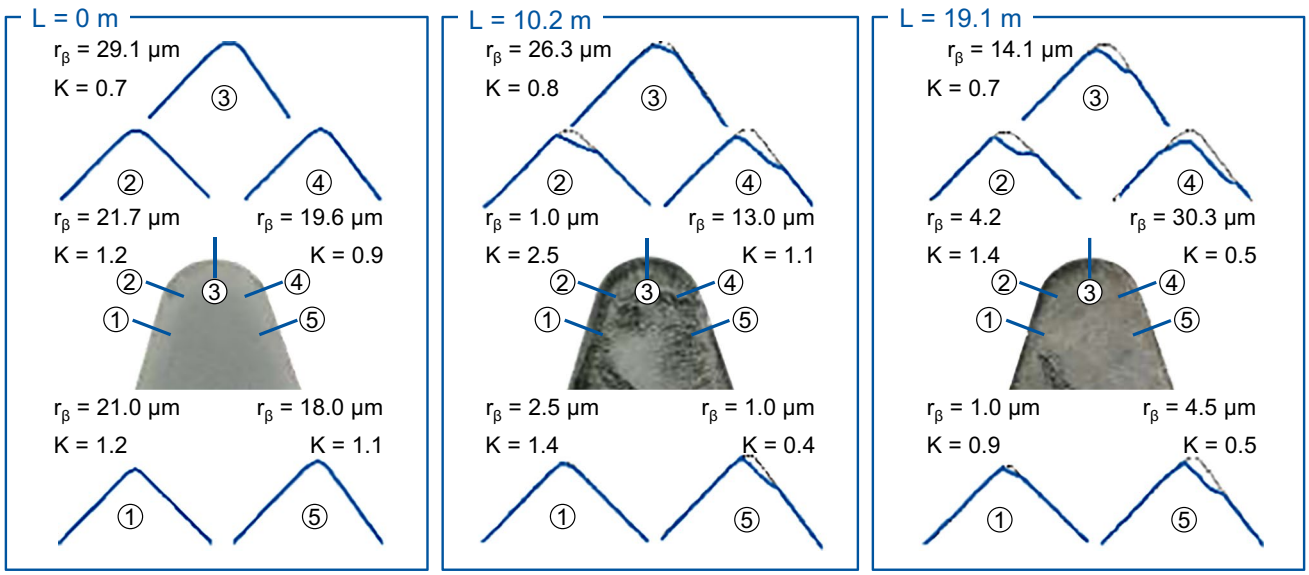

Fig. 11 Cutting edge geometry after defined machined lengths at the tool with $r_\beta = 22$ µm and $K = 1$

After reaching the end of the tool life at $L = 19.1$ m, the cutting edge offset is even more visible at all positions. The radii remain very low at all positions with the exception of position 4, where the radius increases. Here a superposition of flank and crater wear occurred.

Figure 12 shows the wear appearance after reaching the wear criterion of the fly-cutters with $K = 1$ and $r_\beta = 30$ µm. SEM micrographs of the leading flank, the tip area, and the trailing flank are shown.

Material adhesion can be seen on the rake face and on the flank. The tool profile is clearly worn over the entire flank. In [29], it was shown that wear on the cutting edge of the tool is cyclical. The adhesion of the material to the cutting edge facilitates increased abrasion. The resulting coating delamination leads to adhesion of the new material again [29]. The cutting edge was reset along the entire tool profile due to flank wear. Crater wear only occurred on the rake face in the transition from the trailing flank to the tip area. In this area, however, the crater wear was formed from the cutting edge towards the center of the rake face, as a result of which the cutting edge was also reset on the rake face due to crater wear. The wear along the tool profile was similar

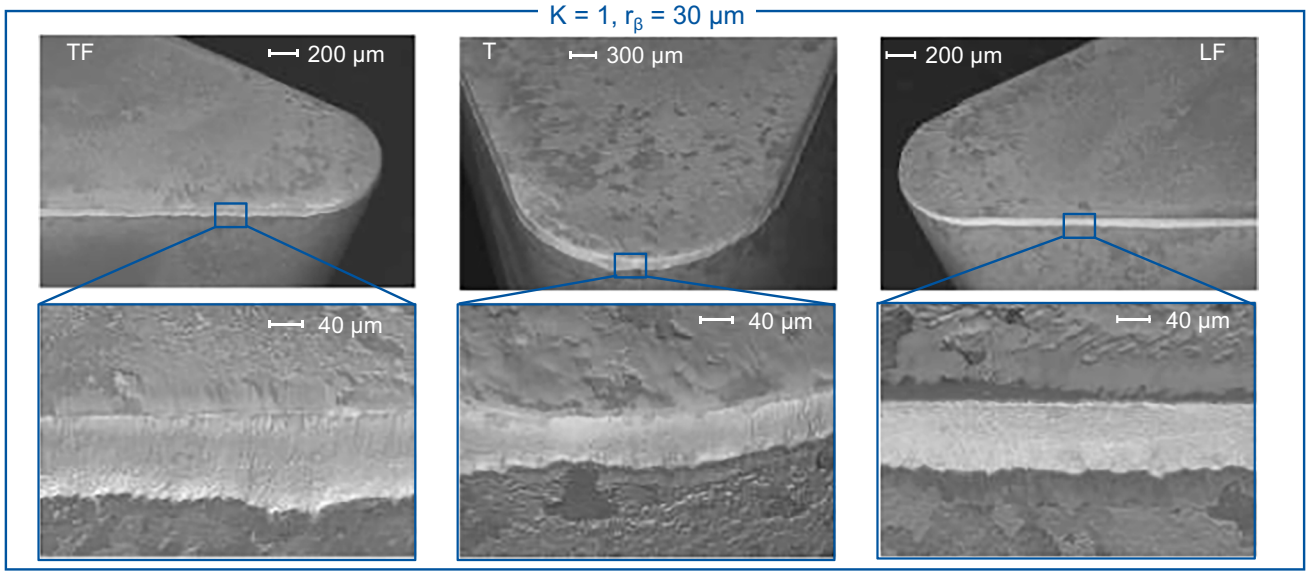

Fig. 12 SEM micrographs of the fly-cutters with a cutting edge radius $r_\beta = 30$ µm

for all cutting edge radii. Therefore, no influence of the cutting edge radius on the wear behavior could be shown on the wear images. Overall, no influence on the wear behavior could be identified by varying the cutting edge radius. The analysis of the wear curves and the wear images could not reveal any clear differences. All tests showed an offset of the cutting edge with the occurrence of flank wear and thus the formation of a new cutting edge with a small cutting edge radius. The same behavior can be related to the fact that all test results showed an offset of the cutting edge when flank wear occurred, resulting in the formation of a new cutting edge with a small cutting edge radius.

3.3 Influence of the form-factor K on the wear behavior

To analyze the influence of the form-factor K on the wear behavior, three fly-cutters were examined. They were prepared with a symmetrical microgeometry ($K=1$) and two asymmetrical microgeometries, one displaced to the rake face ($K<1$) and one to the flank ($K>1$). After the coating process, the fly-cutter was classified into $K=0.3$, $K=1$, and $K=3$. The target value for the cutting edge radius was $r_\beta=18$ µm for all tools. The prepared and coated state of the fly-cutter was documented with the help of SEM micrographs and compared in Fig. 13. The images show the leading and trailing flanks of each fly-cutter.

The different tool microgeometries of the cutting edge can be seen in the SEM micrographs. In the case of the fly-cutter with $K=0.3$, the cutting edge is displaced towards the rake face, in the case of the fly-cutter $K=1$, there is a symmetrical cutting edge, and in the case of the tool with $K=3$, the cutting edge is displaced towards the clearance face. The cutting edge of all tools is homogeneously and defect-free prepared along the tool profile. Figure 13 shows partially small coating defects in the form of small white dots on the rake and clearance surfaces. However, the tool defects did not occur over a large area and only with a low frequency. Therefore, the tools from the respective batches were used in the trials.

The wear behavior of the fly-cutters with different form-factors is shown in Fig. 14. All tools reached the wear criterion by flank wear at TF-A. The fly-cutter with a form-factor of $K=3$ reached the wear criterion after $N=13$ workpieces, which corresponds to a tool life of LT = 16.5 m. Using the fly-cutters with $K=1$ and $K=0.3$, $N=14$, workpieces could be machined before the wear criterion was reached, which corresponds to a tool life of LT = 17.8 m. In the wear-critical area AF-A, differences can be seen in the course of the maximum flank wear. The higher the form-factor K, the higher the initial wear. The stable operating phase (linear range) is reached earlier but also with a higher initial wear. The slope of the linear range is comparable between the tools. All fly-cutters reached the exponential wear range after a comparable machined length. Crater wear occurred with all tools on the rake face at TF-A, which however did not lead to tool failure. Cutting edge chipping did not occur in the trials.

For the two fly-cutters with the biggest difference in microgeometry, $K=0.3$ and $K=3$, SEM micrographs of the leading flank, the tip area, and the trailing flank were taken after the wear criterion was exceeded, see Figs. 15 and 16. On both fly-cutters, material adhesion can be seen on the rake and clearance surfaces. The flank wear of both tools occurred continuously along the entire tool profile. The

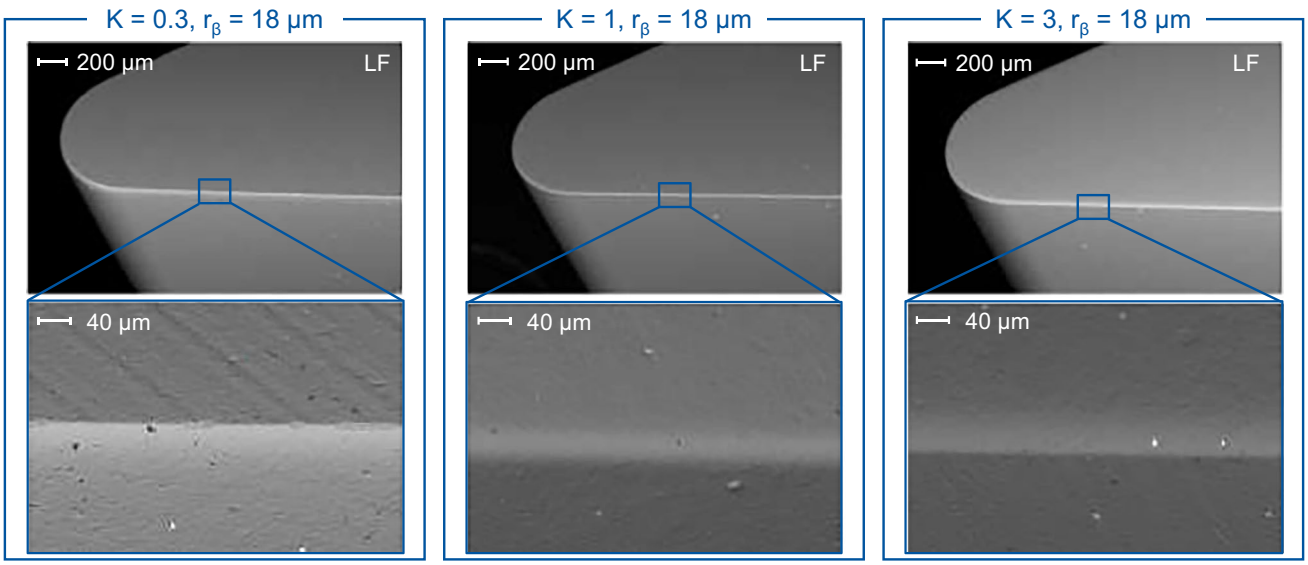

Fig. 13 Initial condition of the fly-cutters with different form-factors K

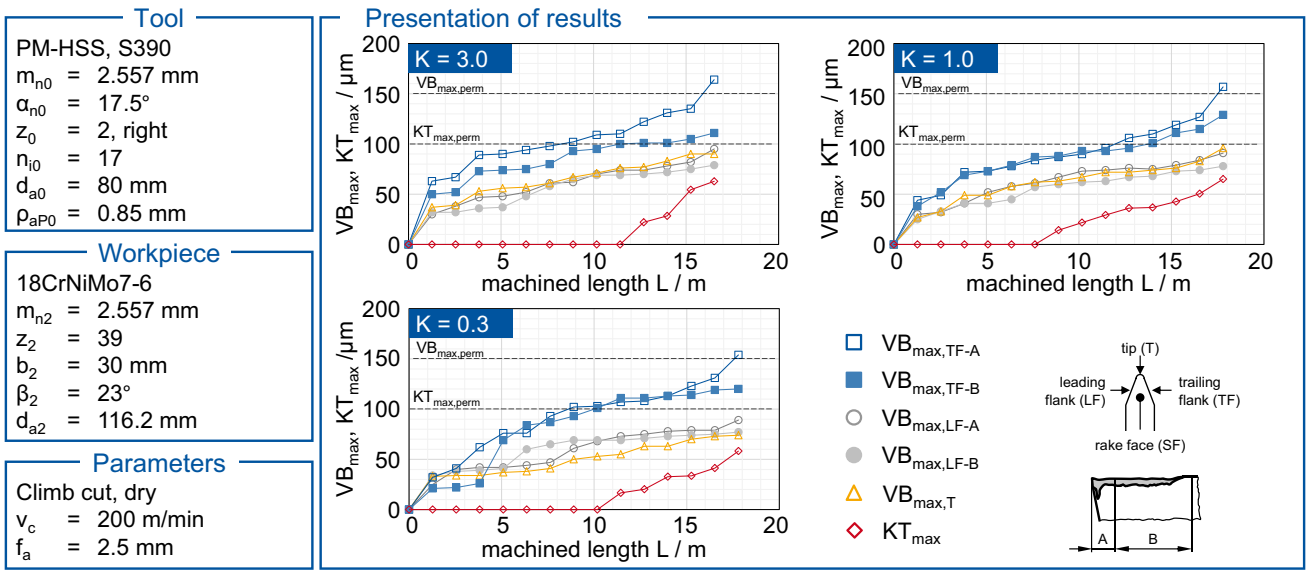

Fig. 14 Wear curves for variation of the form-factor K

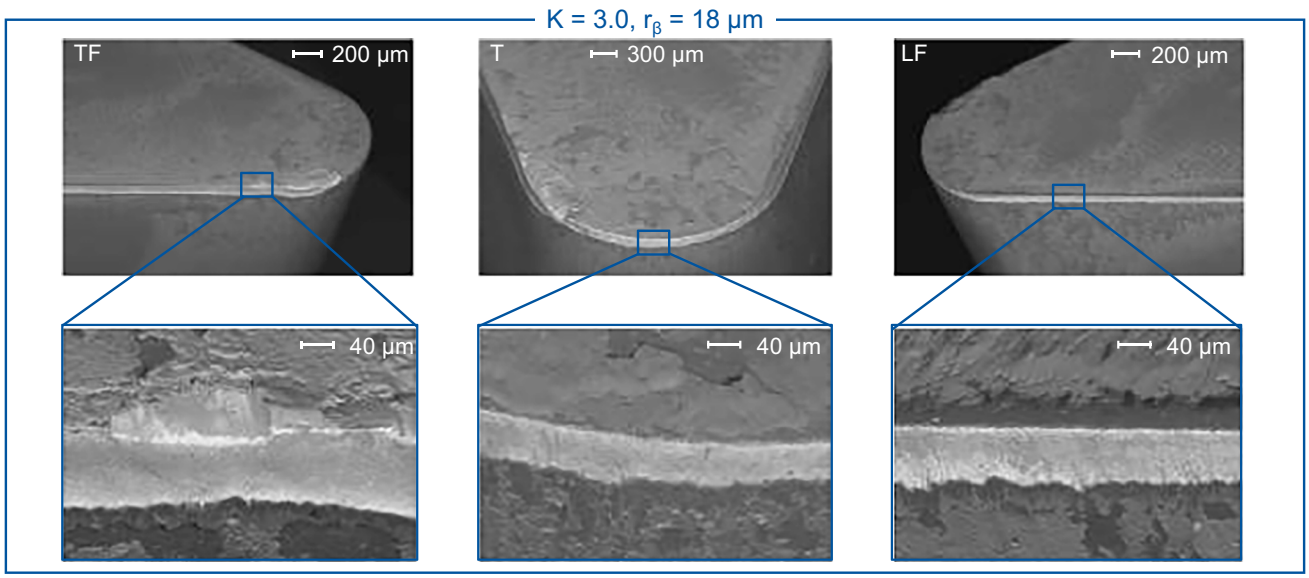

Fig. 15 SEM images of the tool with the form-factor $K=3$

cutting edge was set back along the entire tool profile due to flank wear. Surface breakage on the rake face did not occur. No major differences in the forms and amounts of wear were apparent between the two tools.

In addition to the described fly-cutting trials, further fly-cutters were used in the design of experiments. The achieved tool life is shown in Fig. 17. The largest tool life with LT = 20.3 m was achieved with a tool microgeometry of $r_\beta = 10$ µm and $K = 1$.

In general, the best results were achieved with a symmetrical cutting edge ($K = 1$). The initial wear was the lowest regarding all test points, and the range of linear wear growth was the longest with a low gradient. With a high form-factor of $K = 3$, 7–25% shorter tool lives were achieved. This is mainly due to the fact that the slope in the linearly growing wear section was higher and thus no stable cutting edge was formed. A small form-factor with $K = 0.3$ could only be produced for small cutting edge radii due to limitations resulting from the manufacturing process. For the trial point with a cutting edge radius of $r_\beta = 10$ µm, a smaller tool life was achieved with a low form-factor $K = 0.3$. For a radius of $r_\beta = 18$ µm, this effect could not be

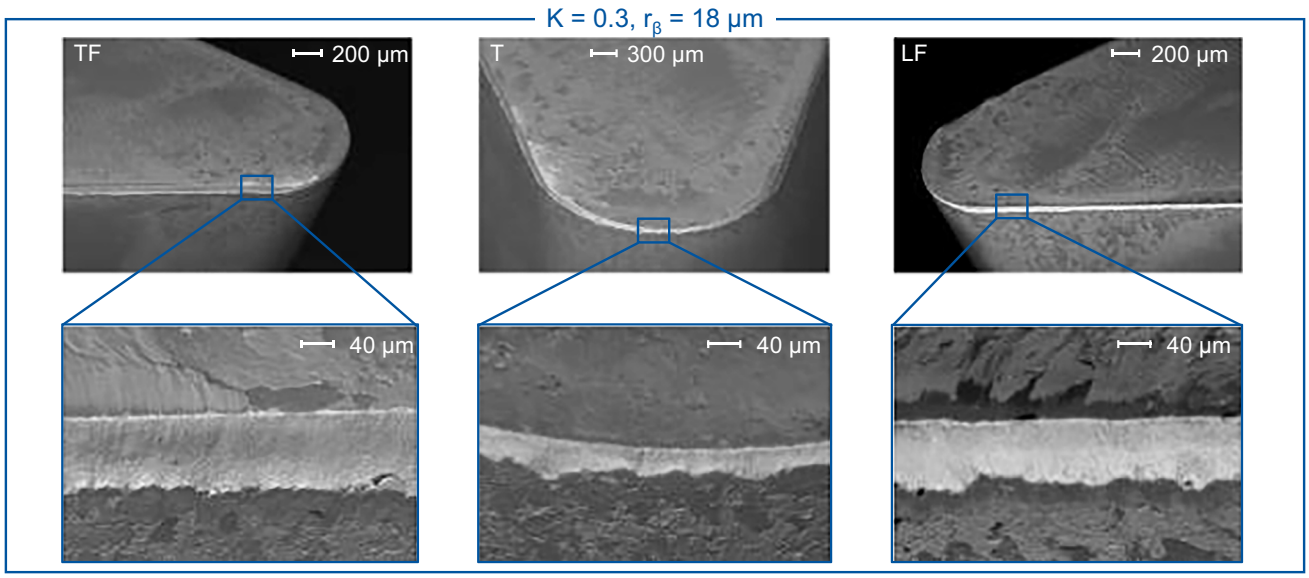

Fig. 16 SEM images of the tool with the form-factor $K = 0.3$

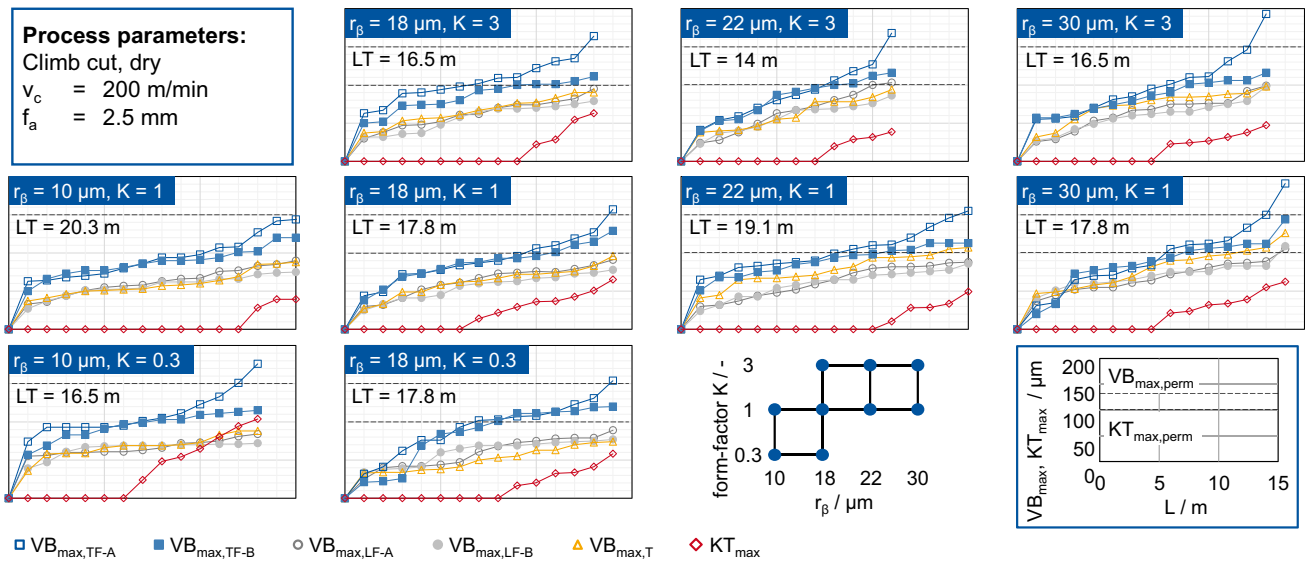

Fig. 17 Summary of all wear curves for micro geometry variation

proven. An influence of the cutting edge radius on the wear behavior could not be verified by the trials.

In summary, the variation of the form-factor has shown a small influence on the wear behavior along the machined length. The tools with a high form-factor $K = 3$ reached the shortest tool life until the wear criterion was exceeded. The fly-cutters with the low form-factor achieved shorter or similar tool lives than the tools used with a symmetrical cutting edge ($K = 1$). An influence of the cutting edge radius on the wear behavior could not be identified.

4 Summary and outlook

The influence of the cutting edge geometry was analyzed in fly-cutting trials. For this purpose, PM-HSS tools with a normal module of $m_{n0} = 2.557$ mm with constant, industry-standard process parameters were used. The cutting velocity was $v_c = 200$ m/min and the axial feed with $f_a = 2.5$ mm for all trials. The workpieces made of 18CrNiMo7-6 were machined without cooling lubricant. The cutting edge radius was varied in the steps $r_\beta = 10$ µm, $r_\beta = 18$ µm,

$r_\beta = 22$ µm, and $r_\beta = 30$ µm and the form-factor in the steps $K = 0.3$, $K = 1$, and $K = 3$. The variation of the form-factor showed a minor influence on the wear behavior of the fly-cutters. The tools with a high form-factor $K = 3$ achieved the shortest tool life. Fly-cutters with a low form-factor $K = 0.3$ achieved shorter to similar tool lives than tools with a symmetrical cutting edge form-factor $K = 1$. An asymmetric cutting edge resulted in higher initial wear or a shorter or more increasing linear wear growth range. Overall, tool lives of $LT \geq 14$ m could be achieved. An influence of the cutting edge radius on the wear behavior could not be identified. The cutting edge was reset by flank wear in all trials. The influence of the preparation process on the wear behavior was mainly attributed to the coating thickness distribution. In this context, it was shown that a sufficient and uniform coating thickness is of fundamental importance for good wear protection.

For the results presented in this report, the experimental data basis will have to be increased in the future so that the identified effects can be statistically verified. Furthermore, the tool microgeometry in the form of cutting edge radius and form-factor must be further investigated in future work. In particular, the machining of the common gear materials 16MnCr5, C45, and 42CrMo4 with PM-HSS tools with and without the use of cooling lubricant holds great potential for increasing tool performance. The investigation of alternative cutting materials such as carbide or Fe-Co-Mo also suggests high potential. With a larger database, the cutting edge geometry of the tools can be designed in a process-oriented manner in the future, and longer tool lives can be achieved.

Acknowledgments The authors gratefully acknowledge the German Federation of Industrial Research Associations for providing the financial support for the project IGF-No. 19704 N based on a resolution of the German Parliament.

Author contribution All authors contributed to the study conception and design. Material preparation, data collection, and analysis were performed by Felix Kühn. The first draft of the manuscript was written by Felix Kühn and Steffen Hendricks, and all authors commented on the previous versions of the manuscript. All authors read and approved the final manuscript.

Funding Open Access funding enabled and organized by Projekt DEAL. This work was supported by the German Federation of Industrial Research Associations, which financially supports the project IGF-No. 19704 N based on a resolution of the German Parliament.

Declarations

Competing interests The authors declare no competing interests.

References

1. Al-Zkeri I, Rech J, Altan T, Hamdi H, Valiorgue F (2009) Optimization of the cutting edge geometry of coated carbide tools in dry turning of steels using a finite element analysis. Mach Sci Technol 13(1):36–51. https://doi.org/10.1080/10910340902776051
2. Bassett E, Köhler J, Denkena B (2012) On the honed cutting edge and its side effects during orthogonal turning operations of AISI1045 with coated WC-Co inserts. CIRP J Manuf Sci Technol 5(2):108–126. https://doi.org/10.1016/j.cirpj.2012.03.004
3. Bergmann B, Grove T (2018) Basic principles for the design of cutting edge roundings. CIRP Ann 67(1):73–78. https://doi.org/10.1016/j.cirp.2018.04.019
4. Bergs T, Brimmers J, Georgoussis A, Krömer M (2021) Investigation of the chip formation during hobbing by means of an analytical approach. Procedia CIRP 99:226–231. https://doi.org/10.1016/j.procir.2021.03.033
5. Bouzakis K-D, Lili E, Michailidis N, Friderikos O (2008) Manufacturing of cylindrical gears by generating cutting processes. A critical synthesis of analysis methods. CIRP Ann Manuf Technol 57(2):676–696
6. Bouzakis K-D, Klocke F, Skordaris G, Bouzakis E, Gerardis S, Katirtzoglou G, Makrimallakis S (2011) Influence of dry microblasting grain quality on wear behaviour of TiAlN coated tools. Wear 271(5–6):783–791. https://doi.org/10.1016/j.wear.2011.03.010
7. Coelho RT, Silva LR, Braghini A, Bezerra AA (2004) Some effects of cutting edge preparation and geometric modifications when turning INCONEL 718™ at high cutting speeds. J Mater Process Technol 148(1):147–153. https://doi.org/10.1016/j.jmatprotec.2004.02.001
8. Deng B, He Q, DePaiva JM, Veldhuis SC (2022) A novel approach to cutting tool edge design based on initial wear stage. J Mater Process Technol 304:117561. https://doi.org/10.1016/j.jmatprotec.2022.117561
9. Denkena B, Biermann D (2014) Cutting edge geometries. CIRP Ann 63(2):631–653. https://doi.org/10.1016/j.cirp.2014.05.009
10. Denkena B, Lucas A, Bassett E (2011) Effects of the cutting edge microgeometry on tool wear and its thermo-mechanical load. CIRP Ann 60(1):73–76. https://doi.org/10.1016/j.cirp.2011.03.098
11. Denkena B, Köhler J, Breidenstein B, Abrão AM, Ventura C (2014) Influence of the cutting edge preparation method on characteristics and performance of PVD coated carbide inserts in hard turning. Surf Coat Technol 254:447–454. https://doi.org/10.1016/j.surfcoat.2014.07.003
12. Denkena B, Krödel A, Heckemeyer A (2021) Numerical and experimental analysis of thermal and mechanical tool load when turning AISI 52100 with ground cutting edge microgeometries. CIRP J Manuf Sci Technol 35:494–501. https://doi.org/10.1016/j.cirpj.2021.08.006
13. Endres WJ, Kountanya RK (2002) The effects of corner radius and edge radius on tool flank wear. J Manuf Process 4(2):89–96. https://doi.org/10.1016/S1526-6125(02)70135-7
14. Fang N, Wu Q (2005) The effects of chamfered and honed tool edge geometry in machining of three aluminum alloys. Int J Mach

Tools Manuf 45(10):1178–1187. https://doi.org/10.1016/j.ijmachtools.2004.12.003
15. Karpat Y, Özel T (2008) Mechanics of high speed cutting with curvilinear edge tools. Int J Mach Tools Manuf 48(2):195–208. https://doi.org/10.1016/j.ijmachtools.2007.08.015
16. Karpuschewski B, Knoche H-J, Hipke M, Beutner M (2012) High performance gear hobbing with powder-metallurgical high-speed-steel. Procedia CIRP 1:196–201. https://doi.org/10.1016/j.procir.2012.04.034
17. Karpuschewski B, Beutner M, Köchig M, Härtling C (2017) Influence of the tool profile on the wear behaviour in gear hobbing. CIRP J Manuf Sci Technol 18:128–134. https://doi.org/10.1016/j.cirpj.2016.11.002
18. Karpuschewski B, Beutner M, Köchig M, Wengler M (2017) Cemented carbide tools in high speed gear hobbing applications. CIRP Ann 66(1):117–120. https://doi.org/10.1016/j.cirp.2017.04.016
19. Kühn F, Löpenhaus C, Brimmers J, Klocke F, Bergs T (2020) Analysis of the influence of the effective angles on the tool wear in gear hobbing. Int J Adv Manuf Technol 108(7–8):2621–2632. https://doi.org/10.1007/s00170-020-05499-0
20. Lux S (1997) Einfluß von Oberflächenstrukturen auf den Verschleiß von Verzahnwerkzeugen aus Schnellarbeitsstahl. Zugl.: Aachen, Techn. Hochsch., Diss., 1997
21. Norm (2013) Metallic materials - conversion of hardness values (ISO 18265:2013)
22. Özel T (2009) Computational modelling of 3D turning: influence of edge micro-geometry on forces, stresses, friction and tool wear in PcBN tooling. J Mater Process Technol 209(11):5167–5177. https://doi.org/10.1016/j.jmatprotec.2009.03.002
23. Ozturk S, Altan E (2012) A slip-line approach to the machining with rounded-edge tool. Int J Adv Manuf Technol 63(5–8):513–522. https://doi.org/10.1007/s00170-012-3941-6
24. Özel T, Ulutan D (2014) Effects of machining parameters and tool geometry on serrated chip formation, specific forces and energies in orthogonal cutting of nickel-based super alloy Inconel 100. Proc Inst Mech Eng B: J Eng Manuf 228(7):673–686. https://doi.org/10.1177/0954405413510291
25. Özel T, Karpat Y, Srivastava A (2008) Hard turning with variable micro-geometry PcBN tools. CIRP Ann 57(1):73–76. https://doi.org/10.1016/j.cirp.2008.03.063
26. Rech J (2006) Influence of cutting edge preparation on the wear resistance in high speed dry gear hobbing. Wear 261:505–512
27. Sari D, Klocke F, Löpenhaus C (2015) Gear finish hobbing: potentials of several cutting materials. Prod Eng Res Devel 9(3):367–376. https://doi.org/10.1007/s11740-015-0626-7
28. Shintani K, Ueki M, Fujimura Y (1989) Optimum tool geometry of CBN tool for continuous turning of carburized steel. Int J Mach Tools Manuf 29(3):403–413. https://doi.org/10.1016/0890-6955(89)90009-6
29. Sousa VF, Silva F, Alexandre R, Fecheira JS, Silva F (2021) Study of the wear behaviour of TiAlSiN and TiAlN PVD coated tools on milling operations of pre-hardened tool steel. Wear 476:203695. https://doi.org/10.1016/j.wear.2021.203695
30. Stein S, Lechthaler M, Krassnitzer S, Albrecht K, Schindler A, Arndt M (2012) Gear Hobbing. A contribution to analogy testing and its wear mechanisms. Procedia CIRP 1:220–225. https://doi.org/10.1016/j.procir.2012.04.039
31. Troß N, Brimmers J, Bergs T (2021) Tool wear in dry gear hobbing of 20MnCr5 case-hardening steel, 42CrMo4 tempered steel and EN-GJS-700–2 cast iron. Wear 476:203737. https://doi.org/10.1016/j.wear.2021.203737
32. Ventura CEH, Chaves HS, Campos Rubio JC, Abrão AM, Denkena B, Breidenstein B (2017) The influence of the cutting tool microgeometry on the machinability of hardened AISI 4140 steel. Int J Adv Manuf Technol 90(9–12):2557–2565. https://doi.org/10.1007/s00170-016-9582-4
33. Winkel O (2004) Steigerung der Leistungsfähigkeit von Hartmetallwälzfräsern durch eine optimierte Werkzeuggestaltung. Zugl.: Aachen, Techn. Hochsch., Diss
34. Wyen C-F, Wegener K (2010) Influence of cutting edge radius on cutting forces in machining titanium. CIRP Ann 59(1):93–96. https://doi.org/10.1016/j.cirp.2010.03.056